J Mater Sci (2009) 44:4653–4660
DOI 10.1007/s10853-009-3712-4

Structure and microstructure of leached Raney-type Al–Ni powders

U. Dahlborg · C. M. Bao · M. Calvo-Dahlborg · F. Devred · B. E. Nieuwenhuys

Received: 27 March 2009 / Accepted: 26 June 2009 / Published online: 17 July 2009

Abstract The structure and microstructure of some leached Raney-type Al–Ni alloys of different compositions have been investigated by neutron diffraction and by small-angle neutron scattering. It was found that all alloys contain a crystalline face-centred cubic (fcc) Ni phase as well as an Al_3Ni_2 phase, the amount of which is decreasing with increasing Al content of the initial alloy. Both the Ni and the Al_3Ni_2 phases are conjectured to be non-stoichiometric. There is no indication of any other crystalline phase. The size of the Ni crystallites in all leached alloys has been found to be of the order of 30 Å, whereas the size of the Al_3Ni_2 ones varies with initial alloy composition and is found to be in the range of 100–250 Å. The change in structure by doping the initial alloys with small amounts of Ti and Cr is after leaching marginal.

Introduction

The results presented below have been obtained within the *IMPRESS Integrated Project* of the EU 6th Framework Program. One of the aims of the project is to develop efficient and cheap Raney-type catalysts [1]. These materials are used for a wide range of catalytic reactions, most notably hydrogenation reactions. In general, Raney-type catalysts are very finely divided powders prepared by grinding an ingot to a fine powder and by chemically dissolving and removing non-active metals from the alloy. With regard to Al–Ni-based alloys, traditional research focuses on the production of powders by casting-and-crushing, and a subsequent leaching process in a concentrated Na(OH) solution after which mainly nanometre-sized metallic Ni particles in a form known as "skeletal" or "sponge" nickel catalyst remains. The process does not only remove most of the aluminium, but it also generates hydrogen gas that serves to activate the nickel catalyst. Raney-type nickel catalysts are extremely pyrophoric due to the small size of the metallic crystallites and the entrapped hydrogen. The relevant chemical reaction can schematically be written [2, 3]:

$$2(\mathrm{Al{-}Ni})_{(s)} + 2\mathrm{OH}^- + 6\mathrm{H_2O} \rightarrow 2\mathrm{Ni} + 2\mathrm{Al(OH)}_{4^-(aq)} + 3\mathrm{H}_{2(g)} \quad (1)$$

Recently, new processing routes, such as multilayer coatings [4], direct spraying [5, 6], rapid solidification [7–11], ball-milling [12, 13], different kinds of chemical activation [14, 15] as well as impulse [16] and gas atomization [1], have been utilized to produce new alloys that after leaching are, or might be, more efficient in catalysis processes and/or in fuel cell applications than the ones obtained by ingot grinding. In the IMPRESS project, the gas atomization technique has been selected as the most promising one in order to produce Al–Ni-based powders suitable for obtaining an efficient Ni catalyst. In the gas atomization process, the disruption of the bulk liquid melt to produce droplets relies on the large velocity difference between the melt and the gas ejected from two nozzles. Amorphous and crystalline powders with powder grain sizes ranging from <1 to about 500 μm are simultaneously produced with this technique. By convenience in the following we will use equivalently the terms "powder

U. Dahlborg · C. M. Bao · M. Calvo-Dahlborg (✉)
GPM, CNRS-UMR6634, University of Rouen, B.P. 12,
76801 Saint-Etienne du Rouvray Cedex, France
e-mail: Monique.Calvo-Dahlborg@univ-rouen.fr

F. Devred · B. E. Nieuwenhuys
Leiden Institute of Chemistry, Leiden University,
Einsteinweg 55, 2333 CC Leiden, The Netherlands

grain" and "grain" to describe a solidified droplet. In order to study the effect of grain size on the structure, the produced powders were sieved into different-sized families. As an example, the family "53-75" means a powder size in the interval [53;75[, thus 53 μm ≤ grain size < 75 μm. Several experimental studies on the catalytic efficiency of Al–Ni-based alloys have been published [8–11, 17–19]. An attempt to model the leaching process has furthermore recently been presented [20].

A lot of study has been devoted to the leaching process, e.g. in Al–Ni alloys of the 50–50 wt% composition ($Al_{68.5}Ni_{31.5}$ at.%). However, the structure and microstructure of leached powders are nevertheless still not well understood. Moreover, many different production routes to obtain the initial alloys have been used, and when comparing published studies it is found that the phase content as well as the composition of the different initial alloys varies considerably from study to study. Thus, as the solidification paths are not the same in these different studies it is difficult to obtain a unified picture of the physical and chemical phenomena occurring during the process and to interpret the origin for the different catalytic efficiencies in various specific reactions. Considering nickel catalysts based on Al–Ni initial alloys, the leaching process has been suggested to proceed through several different routes involving different intermediate phases [8, 21]. However, in most of these studies the state and the phase content of the initial material have not been accurately known. Without such a detailed knowledge, a description of the leaching process is more of less hypothetical.

In this article, a structural characterization of some binary and ternary Al–Ni alloys after leaching is presented. The structure of gas-atomized Al–Ni-based powders of several different compositions and in different grain size ranges has earlier been determined by neutron and X-ray diffraction [22] as well as by atom probe tomography [23]. It was found that the volume fractions of the three main phases (Al_3Ni, Al_3Ni_2 and Al) present in a powder grain vary with grain size. Comparison between the X-ray and neutron diffraction (ND) results has furthermore revealed that the shell of a powder grain contains more of the Al_3Ni_2 phase than the bulk. Recently, the catalytic performance for a specific catalysis reaction was determined for some powder compositions and grain sizes [19]. It was found that the catalytic activity is very sensitive to the initial alloy composition and it was increasing with the amount of the Al_3Ni phase in the starting alloy. It was furthermore found that adding a low amount (around 2 at.%) of a third metal as a promoter in some cases increases the catalytic efficiency.

The compositions of the three initial binary Al–Ni-based powders investigated in this study are all on the Al-rich side of the phase diagram. When expressed in at.% the compositions are $Al_{75}Ni_{25}$, $Al_{68.5}Ni_{31.5}$ and $Al_{60}Ni_{40}$. The $Al_{68.5}Ni_{31.5}$ alloy corresponds to the 50–50 Al–Ni wt% composition and is traditionally used for industrial production of Raney-type nickel catalysts. The nomenclature used in this article is to specify alloy compositions in per cent as indices and the different phases according to their chemical formula. The structure after leaching of Al–Ni alloys doped with small amounts of Ti and Cr is also presented as well as the first preliminary results on the microstructure of one alloy after leaching as obtained by small-angle neutron scattering (SANS). The phase content of the initial gas-atomized powders as determined by ND is given in Table 1 [22]. Three phases are always present: Al_3Ni, Al_3Ni_2 and elemental Al. Furthermore, the Ti-containing powders were found to contain a weight fraction of about 2% of the Al_3Ti phase that though is not included in Table 1. Moreover, in small grain powders (<200 μm) an additional metastable phase is present in an amount that increases with decreasing powder grain size [22, 23].

Experimental details

Sample preparation: the leaching process

The various Ni–Al precursor alloys were treated with an excess of aqueous 20 wt% sodium hydroxide solution. This excess of concentrated sodium hydroxide (>10 wt%) is required to avoid the precipitation of bayerite which can block the pores of the catalyst by covering the nickel

Table 1 Initial phase weight fractions (wt%) of the investigated powders [20] by ND and by SANS. The binary powders contain a small amount of an additional metastable phase of unknown composition not listed in the table

Exp. technique	Powder composition	Grain size range (μm)	Al_3Ni	Al_3Ni_2	Al
ND	$Al_{60}Ni_{40}$	53–75	~0	~100	~0
	$Al_{68.5}Ni_{31.5}$	53–75	38.1 ± 0.6	55.1 ± 0.6	6.8 ± 0.5
	$Al_{75}Ni_{25}$	53–75	50.3 ± 0.5	34.3 ± 0.4	15.5 ± 0.4
	$Al_{68.5}Ni_{30}Ti_{1.5}$	50–100	36.5 ± 0.6	57.5 ± 0.5	5.5 ± 0.4
	$Al_{68.5}Ni_{30}Ti_{0.75}Cr_{0.75}$	50–100	29.5 ± 0.6	62.0 ± 0.6	8.1 ± 0.4
	$Al_{68.5}Ni_{30}Cr_{1.5}$	50–100	37.4 ± 0.6	55.8 ± 0.6	6.8 ± 0.5
SANS	$Al_{75}Ni_{25}$	106–150	52.9 ± 0.5	32.7 ± 0.3	14.4 ± 0.3

surface [2]. An aliquot of 5 g of powder sample was slowly introduced into 300 mL sodium hydroxide solution at 50 °C. Due to the exothermic reaction, the temperature increased quickly to about 80 °C, which was kept constant during the reaction. After 3 h, the reaction was considered to be completed as no hydrogen gas evolved anymore. The sodium hydroxide was then removed and the powder sample was washed six times with 150 mL of distilled water. The samples were stored immersed in water to avoid exposure to air and washed with heavy water prior to ND experiments.

Neutron diffraction

The ND measurements were performed on the HRPT diffractometer at the Swiss neutron spallation source SINQ [24]. Raney-type nickel catalysts are extremely pyrophoric due to the small size of the metallic crystallites and the hydrogen entrapped in the catalyst pores and should thus not be exposed to oxygen. Accordingly all powders were immersed in heavy water and contained in 8 mm thin-walled cylindrical vanadium cans. The wavelength λ of the neutrons was chosen to 1.494 Å which at a neutron wavevector transfer $Q = 4\pi/\lambda\sin(\theta)$ of 3 $Å^{-1}$ implied a resolution $\Delta Q/Q$ of about 1%, and 2Θ is the scattering angle.

The SANS measurements on one selected leached sample were performed on the SANS-II instrument at the Swiss neutron spallation source SINQ [24]. The leached powder was in this case also kept in heavy water but the diameter of the thin-walled cylindrical vanadium can was 15 mm. The incident neutron wavelength was chosen to 6.4 Å and two sample-detector distances were used, 1 and 5 m, in order to cover as large wavevector transfer as possible. Consequently, the performed SANS measurements could give information on the microstructure of the sample in a size ranging from some tens of Å to about 1000 Å.

Results from ND

One example of a measured diffraction pattern from a leached sample is shown in Fig. 1a. The signal from heavy water in which the leached powder was kept constitutes a major part of the intensity, but diffraction peaks from some remaining crystalline material in the sample are also clearly visible. In order to separate out the water background, one measurement without powder in the filled vanadium can was performed. However, as the relative amount of powder and heavy water is more or less unknown, the measured heavy water background $I(Q)_{\text{water}}$ cannot be directly subtracted from the diffraction pattern measured from powder + water. Thus, another approach

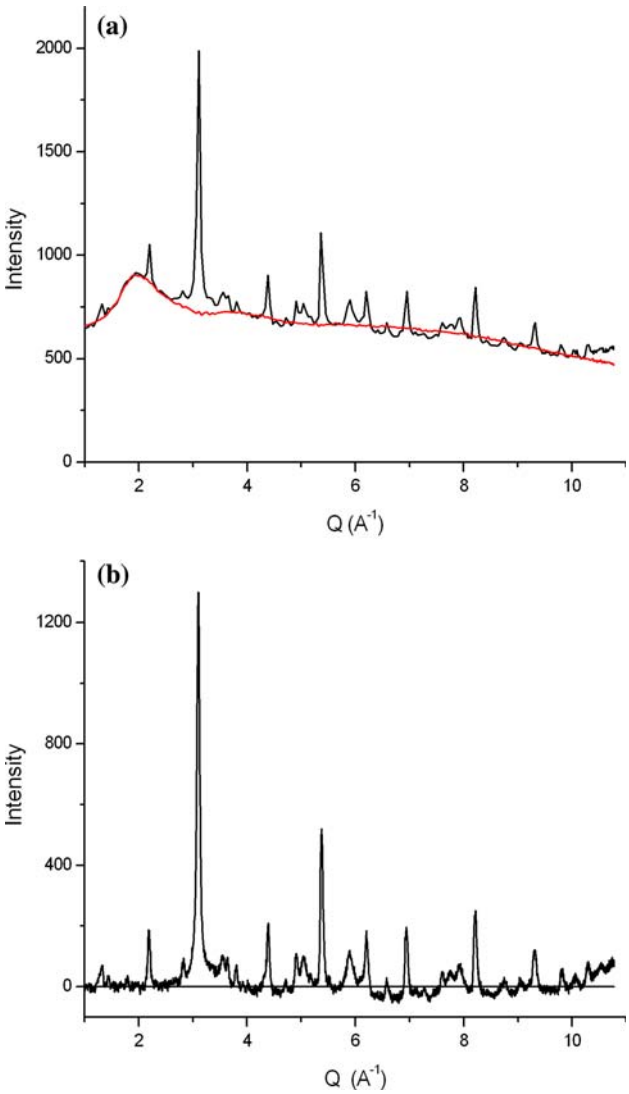

Fig. 1 **a** Measured intensity distribution from an initial $Al_{60}Ni_{40}$ powder leached 30 min and immersed in heavy water. The *flat red curve* shows the intensity contribution from heavy water as obtained by least squares fit in some selected Q ranges. **b** The diffraction pattern in (**a**) after subtraction of the fitted heavy water background. (Color figure online)

was taken in that the measured powder + water patterns were in some selected Q regions fitted by the expression $c_1 * I(Q)_{\text{water}} + c_2 + c_3 * Q^2$. The constants c_2 and c_3 were included to account for the incoherent background originating from the nickel and deuterium nuclei as well as for a possible inelastic scattering component. The Q regions used in the fit were selected where no diffraction peaks could be neither observed nor expected to be present in the measured patterns. The background-corrected diffraction pattern obtained by applying this procedure is shown in Fig. 1b. It can be seen that the obtained pattern is suitable as a basis for a structure-refinement procedure. However, it can also be seen that the procedure does not reproduce the scattering component from heavy water in

full detail in that an oscillating small intensity background seems still to be present. The reason is most probably that the water structure is actually modified by the presence of remaining (Al_3Ni_2) and by created (Ni) particles in the leached alloy as will be discussed below. A hydration structure in an aqueous solution of nickel ions has been seen in earlier studies [25–27]. However, the presence of an oscillating background does not influence the results discussed below to any significant extent as it is properly taken into account by the FullProf computer code [28] used in order to quantitatively analyse the phase content of the leached powders.

Although the leaching of aluminium is initially very fast, a relatively long leaching time (up to 3 h) is required to complete the process [16–19]. In order to study its time dependence, several powders were measured after two leaching times, 30 and 180 min. Figures 2 and 3 show the corresponding measured diffraction patterns obtained after correction for heavy water background for $Al_{60}Ni_{40}$ and $Al_{75}Ni_{25}$ powders of initial grain sizes in the range of 53–75 μm. The diffraction peak positions for possible crystalline inclusions are shown at the bottom of the figure. $NaAl(OH)_4$ is an intermediate phase in the leaching process.

It may be concluded that the $Al_{60}Ni_{40}$ powder after leaching not only contains elemental fcc nickel, but also a substantial amount of other crystalline components. It has earlier been shown that both the elemental Al and the Al_3Ni phases are easily removed in the leaching process,

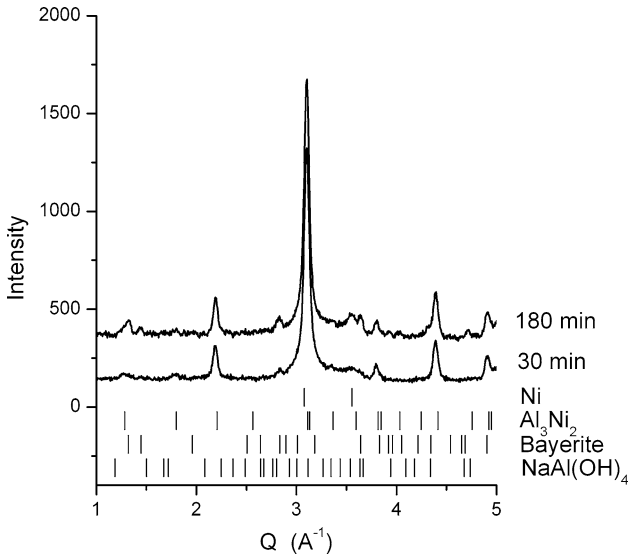

Fig. 2 Diffraction patterns from initial $Al_{60}Ni_{40}$ powders after 30 (*lower curve*) and 180 (*upper curve*) min of leaching. The *vertical line symbols* denote Bragg peak positions for the (from above) Ni, Al_3Ni_2, bayerite and $NaAl(OH)_4$, respectively

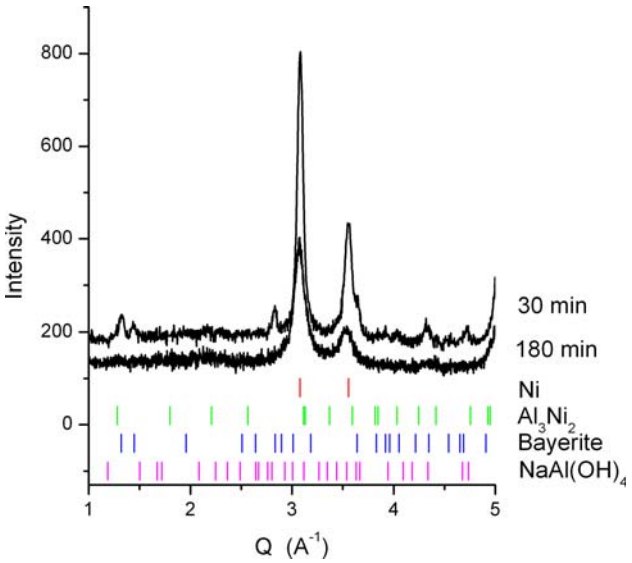

Fig. 3 Diffraction patterns from initial $Al_{75}Ni_{25}$ powders after 30 (*upper curve*) and 180 (*lower curve*) min of leaching. The *vertical line symbols* denote Bragg peak positions for the (from above) Ni, Al_3Ni_2, bayerite and $NaAl(OH)_4$ phases, respectively

and any diffraction peaks from these are accordingly not detected in the diffraction pattern. It is also seen that for the $Al_{60}Ni_{40}$ powder the leaching time does not play an important role as even after 3 h a large amount of the initially present Al_3Ni_2 phase remains. In order to quantify the amount of the different phases, the diffraction patterns were analysed with the FullProf computer code. The obtained weight fraction of the Al_3Ni_2 phase is, as obtained from the refinement, larger than 80% (see Table 2). The derived sizes of Ni and Al_3Ni_2 crystallites are about 35 and 200 Å, respectively, slightly smaller after the longer leaching time. The agreement between the measured and the calculated patterns is satisfactory but it is obvious that another crystalline component is present as indicated by the relatively strong peak at about 2.8 $Å^{-1}$. This peak is found to originate from α-$Al(OH)_3$, bayerite, and to result as mentioned above from an incomplete washing of the powder after the leaching procedure. The bayerite is thus treated as an impurity and it is accordingly not included in the refinement. The intermediate $NaAl(OH)_4$ phase is not present after leaching.

From Fig. 3, it may be concluded that after 30 min of leaching the powder of initial composition $Al_{75}Ni_{25}$ contains mainly elemental fcc nickel, no Al_3Ni phase and only a small amount of Al_3Ni_2 phase. After 3 h the amount of Al_3Ni_2 is very small and close to the detection limit. Bayerite is also present but as was mentioned above is a parasite compound originating from the leaching process. The size of the Ni crystallites is found to be of the order of 120 Å after 3 h of leaching.

Table 2 Derived phase composition and crystallite size of the leached powders as obtained by refinements with the FullProf computer code of the background-corrected measured ND data and from the GIFT computer code of the measured SANS pattern

Exp. technique	Powder composition	Grain size range (μm)	Leaching time (min)	Ni		Al_3Ni_2	
				Weight fraction (%)	Cryst. size (Å)	Weight fraction (%)	Cryst. size (Å)
ND	$Al_{60}Ni_{40}$	53–75	30	16 ± 1	37 ± 1	84 ± 1	199 ± 5
	$Al_{60}Ni_{40}$	53–75	180	15 ± 1	33 ± 2	85 ± 1	176 ± 3
	$Al_{68.5}Ni_{31.5}$	53–75	180	–	–	–	–
	$Al_{75}Ni_{25}$	53–75	30	>90	–	<10	–
	$Al_{75}Ni_{25}$	53–75	180	>90	–	<10	–
	$Al_{68.5}Ni_{30}Ti_{1.5}$	50–100	180	13 ± 3	57 ± 5	77 ± 3	112 ± 3
	$Al_{68.5}Ni_{30}Ti_{0.75}Cr_{0.75}$	50–100	180	17 ± 2	38 ± 3	83 ± 2	108 ± 2
	$Al_{68.5}Ni_{30}Cr_{1.5}$	50–100	180	18 ± 2	–	82 ± 2	97 ± 2
SANS	$Al_{75}Ni_{25}$	106–150	180	–	35 ± 5	–	250 ± 150

Diffraction patterns of the three binary Al–Ni powders after 3 h leaching are shown in Fig. 4. The refinement of the $Al_{68.5}Ni_{31.5}$ diffraction pattern was unfortunately not fully satisfactory because of a large amount of bayerite present in this sample, thus indicating an insufficient rinsing. Accordingly no results for this alloy are included in Table 2. It can be concluded from Table 2 that there is a difference in phase content between the alloys; the higher Al content in the initial parent powders the less crystalline inclusions, i.e. the less of the Al_3Ni_2 phase, it contains after leaching. In all powders there is no sign of Al_3Ni and Al phases, neither of the unidentified phases that are present to a small amount in the initial powders at small grain sizes [22, 23].

The effect of adding a small amount of Ti and/or Cr dopant to a powder based on $Al_{68.5}Ni_{31.5}$ composition is shown in Fig. 5. The diffraction curves are very similar and all powders contain two main crystalline phases: (i) Ni with varying size of the crystallites and (ii) Al_3Ni_2 with a weight fraction about 80%. For the Cr-containing powder, the size as obtained from the refinement is found to be about 100 Å, for the Ti-containing powder about 60 Å and for the powder that contains both Cr and Ti about 40 Å.

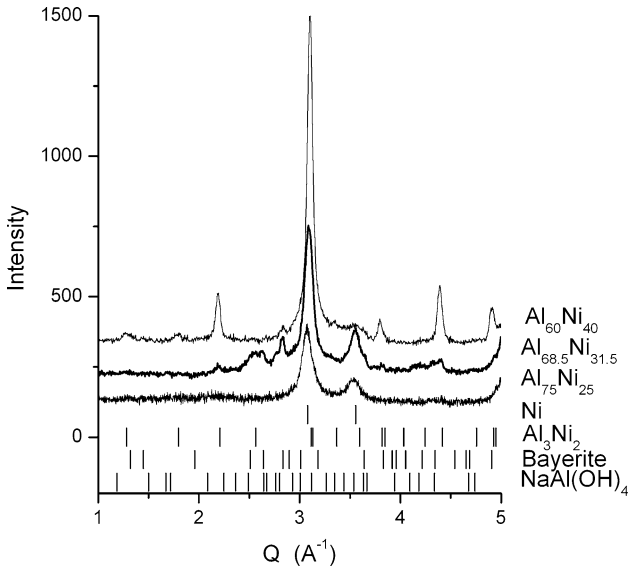

Fig. 4 Diffraction patterns from initial $Al_{60}Ni_{40}$ (*upper curve*), $Al_{68.5}Ni_{31.5}$ (*middle curve*) and $Al_{75}Ni_{25}$ (*lower curve*) initial powders, after 180 min of leaching. The *vertical line symbols* denote Bragg peak positions for (from above) the Ni, Al_3Ni_2, bayerite and $NaAl(OH)_4$ phases, respectively

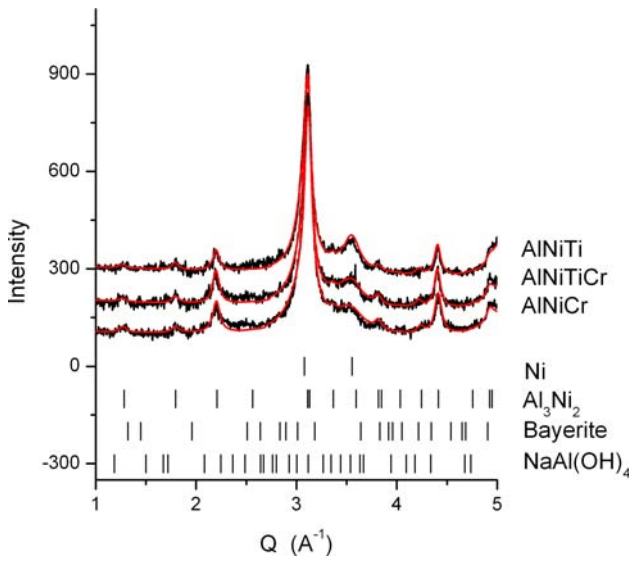

Fig. 5 Diffraction patterns from initial $Al_{68.5}Ni_{30}Cr_{1.5}$ (*lower curve*), $Al_{68.5}Ni_{30}Cr_{0.75}Ti_{0.75}$ (*middle curve*) and $Al_{68.5}Ni_{30}Ti_{1.5}$ (*upper curve*) powders, after 180 min of leaching. The *vertical line symbols* denote Bragg peak positions for (from above) the Ni, Al_3Ni_2, bayerite and $NaAl(OH)_4$ phases, respectively

Results from SANS

SANS occurs because of differences in the scattering properties of a material on a length scale larger than the interatomic spacing. The macroscopic differential scattering cross section which determines the scattered intensity, for a dilute and isotropically scattering system, consisting of N_p identical particles (scattering units) of volume V_p, can be written as [29]:

$$\frac{d\sigma}{d\Omega} = \frac{V_p^2 N_p}{N}(\rho_p - \rho_m)^2 |F_p(Q)|^2 \quad (2)$$

Q is as mentioned above the scattering vector, $F_p(Q)$ is the form factor of the particle (scattering object), ρ_p is the scattering length density (the sum of the neutron scattering lengths of the atomic nuclei in a particle per unit volume) and ρ_m is the corresponding quantity of the surrounding medium. The quantity $(\rho_p - \rho_m)^2$ is called the contrast. Thus, in a SANS experiment the strength of the measured signal is proportional to the contrast and not to the scattering length of the individual nuclei, as is the case in an ordinary diffraction experiment. It should also be noted that there is no small-angle scattering from a homogeneous system. For a system containing several different kinds of particles, as well as with different sizes and shapes, Eq. 2 takes a considerably more complex form. To extract information from a SANS experiment is in this case thus very complicated. It should also be noted that the presence of a pore as well as an interface structure between a particle (scattering unit) and the matrix in a material will also result in a SANS signal.

From the diffraction measurements presented above and from earlier experiences, the investigated leached powders contain particles consisting of Ni and Al_3Ni_2 and possibly also Al_2O_3 and bayerite. As the powder sample is sponge-like it furthermore contains also pores. The relative contrasts for all the microstructural possible scattering units are listed in Table 3. The given values are calculated from nominal compositions. No account has been taken to the non-stoichiometry found to exist in the initial powders [22].

Table 3 Relative contrasts for particles (scattering units) of different composition in air and in heavy water (D_2O)

Particle composition	Relative contrast (%)	
	In air	In D_2O
Ni	42.2	16.6
Al_3Ni_2	9.5	6.0
Al_2O_3	15.5	0.7
$Al(OD)_3$	32.8	6.6
Pore	0	70.0

The leaching of a powder initially of composition $Al_{75}Ni_{25}$ and grain size in the range of 106–150 μm was investigated by SANS. The patterns measured from the parent powder, from the powder immersed in heavy water and from the powder after 3 h of leaching are shown in Fig. 6. A strong signal is observed in all three cases, indicating the inhomogeneity of the sample. In order to obtain the curves in Fig. 6, the incoherent flat background originating from both heavy water and Ni has been subtracted from the measured patterns. However, this procedure is a rather uncertain correction as the relative amounts of heavy water and Ni in the neutron beam are not accurately known. Accordingly, the curves shown in Fig. 6 may have a systematic error with regard to absolute intensity of the order of 10% in the large Q region, whereas in the small Q regions, this uncertainty is negligible. The measured patterns for the non-leached parent powders in Fig. 6 are rather featureless as compared to the ones measured from the leached powders. Nevertheless, both patterns show small irregularities around $Q = 0.05$ Å^{-1}, although of different magnitude for the parent powder and the one immersed in heavy water. As the contrast is different in the two cases (see Table 2), this indicates either a surface contribution to the intensity or the existence of smaller particles at the surface of powder grains that have another composition than the inside of the grain to which they are connected. The relevant length scale for these structural

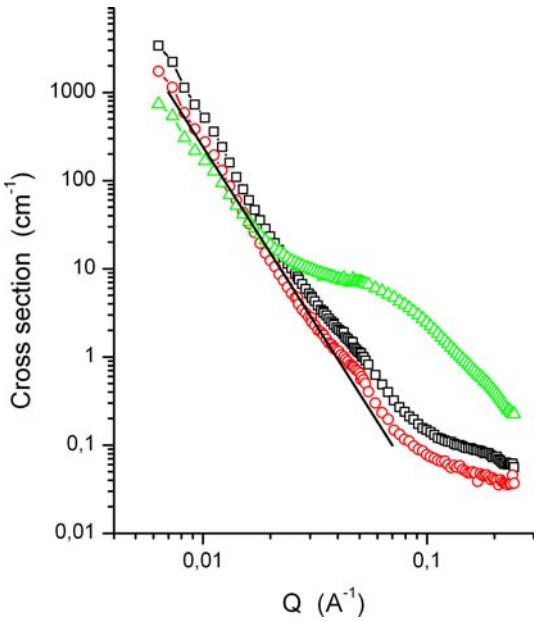

Fig. 6 SANS curves measured from an $Al_{75}Ni_{25}$ powder with powder grain sizes in the range of 106–150 μm. *Black squares curve* parent powder, *red circles curve* powder immersed in heavy water, *green triangles curve* powder after 3 h of leaching. The *line* corresponds to the intensity variation in the Porod limit. (Color figure online)

features is less than about 100 Å. For small Q, the intensity varies in all measurements closely to the Porod law as Q^{-4} [30]. This indicates that the samples on a length scale larger than about 300 Å contain scattering units with a well-defined surface.

In order to obtain more quantitative information on the microstructure, the GIFT computer code [31–33] was used to derive the volume-weighted size distributions shown in Fig. 7 of the scattering units (particle size distribution, PSD) existing in the powders. The areas of all PSDs have been normalized to 10. The results for the non-leached parent powders are similar for small sizes (<600 Å) that, according to the contrasts listed in Table 3, indicates that no small size Al_2O_3 particles exist in the powders and that the peak around 400 Å corresponds to Al_3Ni_2 particles. It can also be concluded that there are no pores in the initial powders in the size range of Fig. 7. Furthermore, there are small peaks around 40 Å, the origin of which presently is uncertain. In the size range above 600 Å, there is a clear difference between the two PSDs. However, as the SANS patterns have been measured in a rather limited small Q range the derivation of a PSD is uncertain in this large size range. The origin of the peaks at about 1000 Å is not understood. The peaks might originate from oxydes, e.g. Al_2O_3.

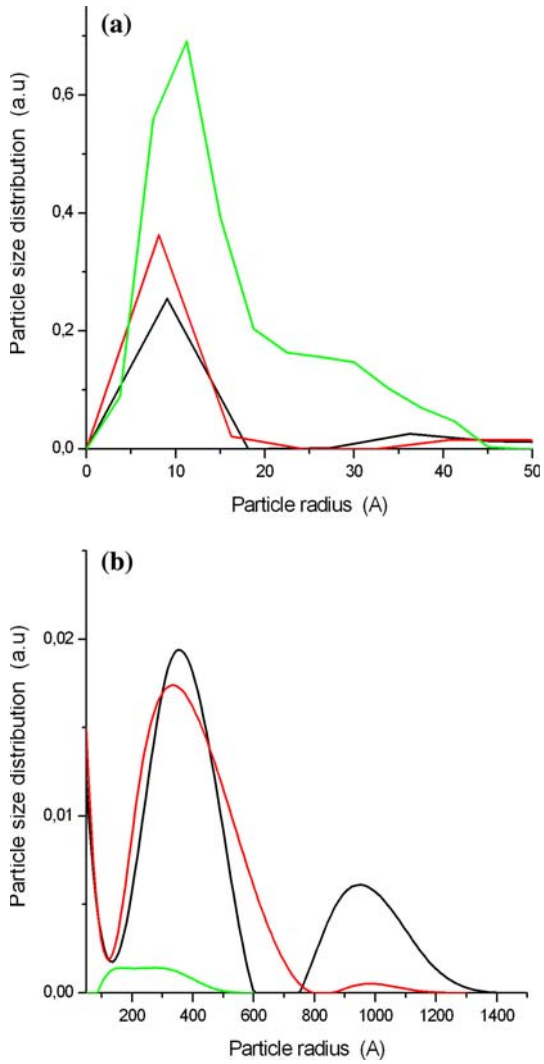

Fig. 7 Volume weighted PSD of an $Al_{75}Ni_{25}$ powder with grain sizes in the range of 106–150 μm in two particle (scattering units) size ranges. *Black curve* (lower in (**a**), upper in (**b**)) parent powder, *red curve* (middle in (**a**) and (**b**)) powder immersed in heavy water, *green curve* (upper in (**a**), lower in (**b**)) powder after leaching during 3 h. (Color figure online)

In the PSD derived for the leached powder, the main contribution is found in a size range smaller than 50 Å but there is also a contribution from Al_3Ni_2 particles remaining after the leaching in the size range of 100–400 Å. The peak at small particle radii consists of two contributions; one centred around 10 and one around 30 Å. As the peak around 10 Å also exists in the non-leached powders it might be due to a small scale microstructure of the powder grain surface. This structure is then more accentuated when a part of the aluminium atoms have been removed during the leaching process. The peak centred around 30 Å very probably corresponds to "pure" Ni particles.

Discussion

The ND measurements of the leached powders presented above have shown that after leaching all samples contain a significant amount of crystalline Ni particles and that all, except the one with $Al_{75}Ni_{25}$ initial composition, also contain a substantial amount of Al_3Ni_2 particles. There is a sign of neither remaining crystalline Al_3Ni and Al phases nor Al_2Ni_3 and Al_2O_3 phases in any leached alloy as has been reported earlier [8, 14]. It is, however, obvious from comparing the weight fractions and the average size of the Al_3Ni_2 particles before and after leaching that they also to a certain extent have been dissolved during the leaching process. This conclusion is supported by the SANS measurements. Thus, the amount of Ni particles in the leached product results both not only from the complete dissolution of Al and Al_3Ni phases, but also to a smaller extent from the dissolution of Al_3Ni_2. The size of the Ni particles was found both from the ND and small-angle measurements to be of the order of 30 Å that is in agreement with other published results [9, 11, 14, 34].

It has recently been found that in small powder grains (<5 μm in diameter) of gas-atomized Al–Ni powders small regions consisting of Al_9Ni_2 phase are present [23]. These regions are too small for a diffraction peak to be created and because of their large Al content they are very probably completely dissolved in the leaching process.

The structural transitions occurring during leaching of a commercial Al_3Ni alloy containing small amounts of Fe

and Cr have recently been investigated [21]. It was concluded from transmission electron microscopy studies that a Ni phase with a crystalline structure corresponding to the Al_3Ni phase co-existed with the fcc Ni phase in the leached alloy. However, no sign of such a phase was observed in this study but instead a small amount of a remaining Al_3Ni_2 phase. In this connection, it has to be mentioned that the lattice parameters as determined from the data refinements presented above showed that the unit cells of both Al_3Ni_2 and Ni phases are larger in the leached alloys than in the initial parent ones. It may thus be conjectured that the Ni phase contains Al atoms, whereas the Al_3Ni_2 phase is non-stoichiometric. It should also be stressed that the treatment of the initial alloys is very different in [21] and in this study. In [21], the initial powder was obtained by grinding a commercial 80–100 μm powder to about 1 μm and in this study the initial powder was produced by gas atomization with grain size of the order of 100 μm.

Conclusions

The ND and the SANS measurements have shown that Al–Ni alloys of initial compositions $Al_{60}Ni_{40}$, $Al_{68.5}Ni_{31.5}$ and $Al_{75}Ni_{25}$ after leaching during 30 and 180 min contain a substantial amount of a crystalline fcc Ni phase as well as an Al_3Ni_2 phase, the amount of which is decreasing with increasing Al content of the initial parent alloy. Both phases are conjectured to be non-stoichiometric. There is no sign of any other Al and/or Ni-based crystalline phase being present. The presence of bayerite in some alloys after leaching has been attributed to insufficient rinsing.

The size of the Ni crystallites in all leached alloys has been found to be of the order of 30 Å, whereas the size of the Al_3Ni_2 ones varies with initial alloy composition and is found to be in the range of 100–250 Å.

The change in structure by doping the initial alloys with small amounts of Ti and Cr is after leaching marginal.

Acknowledgements This study is based on experiments performed at the Swiss spallation neutron source SINQ, Paul Scherrer Institute, Villigen, Switzerland, and has been supported by the European Commission under the 6th Framework Programme through the Key Action: Strengthening the European Research Area, Research Infrastructures, Contract no.: RII3-CT-2003-505925. During the HRPT experiments as well as for the data analysis the authors were very much profiting from the assistance of Denis Sheptyakov and during the measurements on SANS-II the attention of Thomas Geue was very much appreciated. This research is furthermore supported by the IMPRESS Integrated Project (Contract NMP3-CT-2004-500635) that is co-funded by the European Commission in the 6th Framework Programme, the European Space Agency and the Swiss Government.

References

1. Jarvis DJ, Voss D (2005) Mater Sci Eng A 413–414:583
2. Fouilloux P, Martin GA, Renouprez AJ, Moraweck B, Imelik B, Prettre M (1972) J Catal 25:212
3. Smith AJ, Trimm DL (2005) Ann Rev Mater Res 35:127
4. Edelstein AS, Everett RK, Richardson GR, Qadri SB, Foley JC, Perepezko JH (1995) Mater Sci Eng A 195:13
5. Makhlouf SA, Ivanov E, Sumiyama K, Suzuki K (1992) J Alloys Compd 187:L1
6. Vijay M, Selvarajan V (2008) J Mater Process Technol 202:112
7. Warlimont H, Kühn U, Mattern N (1997) Mater Sci Eng A 226–228:900
8. Wang R, Lu Z, Ko T (2001) J Mater Sci 36:5649. doi: 10.1023/A:1012578002418
9. Lei H, Song Z, Tan D, Bao X, Mu X, Zong B, Min E (2001) Appl Catal A 214:69
10. Jobst K, Warlimont H (2002) J Catal 207:23
11. Hu H, Qiao M, Wang S, Fan K, Li H, Zong B, Zhang X (2004) J Catal 221:612
12. Dutta H, Pradhan SK, De M (2002) Mater Chem Phys 74:167
13. Sharafutdinov MR, Korchagin MA, Shkodich NF, Tolochko BP, Tsygankov PA, Yagubova IYu (2007) Nucl Instrum Methods Phys Res A 575:149
14. Petró J, Bóta A, László K, Beyer H, Kálmán E, Dódony I (2000) Appl Catal A 190:73
15. Ham HC, Maganyuk AP, Han J, Yoon SP, Nam SW, Lim TH, Hong SA (2007) J Alloys Compd 446:733
16. Henein H (2002) Mater Sci Eng A 236:92
17. Devred F, Hoffer BW, Sloof WG, Kooyman PJ, van Langeveld AD, Zandbergen HW (2003) Appl Catal A 244:291
18. Hoffer BW, Crezee E, Devred F, Mooijman PRM, Sloof WG, Kooyman PJ, van Langeveld AD, Kapteijn F, Moulijn JA (2003) Appl Catal A 253:437
19. Devred F, Gieske AH, Adkins N, Dahlborg U, Bao CM, Calvo-Dahlborg M, Bakker JW, Nieuwenhuys BE (2009) Appl Catal A Gen 356:154
20. Tong MM, Browne DJ (2008) J Mater Process Technol 202:419
21. Wang R, Chen H, Lu Z, Qiu S, Ko T (2008) J Mater Sci 43:5712. doi:10.1007/s10853-008-2901-x
22. Bao CM, Dahlborg U, Adkins N, Calvo-Dahlborg M (2009) J Alloys Compd 481:199
23. Calvo-Dahlborg M, Chambreland S, Bao CM, Quelennec X, Cadel E, Cuvilly F, Dahlborg U (2008) Ultramicroscopy 109:672
24. http://sinq.web.psi.ch/sinq. Accessed 26 Mar 2009
25. Neilson GW, Enderby JE (1983) Proc R Soc Lond A 390:353
26. Powell DH, Neilson GW, Enderby JE (1989) J Phys Condens Matter 1:8721
27. Howell I, Neilson GW (1997) J Mol Liq 73–74:337
28. http://www.ill.eu/dif/software. Accessed 26 Mar 2009
29. Dahlborg U, Calvo-Dahlborg M, Popel PS, Sidorov VE (2000) Eur Phys J B 14:639
30. Porod G (1982) In: Glatter O, Kratky O (eds) General theory in small-angle x-ray and neutron scattering. Academic Press, London, pp 17–51
31. Glatter O (1977) J Appl Cryst 10:415
32. Brunner-Popela J, Glatter O (1997) J Appl Cryst 30:431
33. Weyerich B, Brunner-Popela J, Glatter O (1999) J Appl Cryst 32:197
34. Bóta A, Goerigk G, Drucker T, Haubold HG, Petró J (2002) J Catal 205:354